Highly Active Porous Carbon-Supported Nonprecious Metal–N Electrocatalyst for Oxygen Reduction Reaction in...

Article *in* The Journal of Physical Chemistry C · April 2010

DOI: 10.1021/jp910138x

CITATIONS
97

READS
352

3 authors, including:

Ja-Yeon Choi
University of Waterloo
28 PUBLICATIONS **1,064** CITATIONS

SEE PROFILE

Zhongwei Chen
University of Waterloo
258 PUBLICATIONS **9,611** CITATIONS

SEE PROFILE

Highly Active Porous Carbon-Supported Nonprecious Metal−N Electrocatalyst for Oxygen Reduction Reaction in PEM Fuel Cells

Ja-Yeon Choi, Ryan S. Hsu, and Zhongwei Chen*

Department of Chemical Engineering, Waterloo Institute for Nanotechnology, Waterloo Institute for Sustainable Energy, University of Waterloo, Waterloo, Ontario, Canada N2L 3G1

Received: October 23, 2009; Revised Manuscript Received: March 30, 2010

As an alternative for platinum to reduce the cost, nonprecious catalysts for the oxygen reduction reaction (ORR) were synthesized by deposition of an Fe/Co−N_x composite onto nanoporous carbon black with ethylenediamine (EDA) as a nitrogen precursor. Two different nanoporous carbon supports, Ketjen Black EC300J (KJ300) and EC600JD (KJ600), were used as catalyst supports for the nonprecious catalysts. Rotating ring disk electrode measurements were carried out to investigate the ORR activity and selectivity of these catalysts. The results obtained from the optimized FeCo/EDA-carbon catalyst, using KJ600 as the support, showed improved onset and half-wave potentials and superior selectivity than that of the KJ300. Similarly, the catalyst showed good performance in the hydrogen−oxygen PEM fuel cell. At a cell voltage of 0.6 V, the fuel cell managed to produce 0.37 A/cm^2 with a maximum power density of 0.44 W/cm^2. A fuel cell life test at a constant voltage of 0.40 V demonstrated promising stability up to 100 h. The catalysts were characterized by X-ray diffraction, energy-dispersive X-ray spectrometry, and X-ray photoelectron spectroscopy. The characterizations indicated that pyridinic-type nitrogen of the nonprecious metal catalysts is critical for ORR catalytic activity and selectivity. These results suggest that a higher pore volume and surface area of the carbon support could lead to a higher nitrogen content, providing more active sites for ORR, and this type of catalyst has great potential used as a nonprecious PEM fuel cell catalyst.

Introduction

Polymer electrolyte membrane (PEM) fuel cells have been receiving lots of attention as a sustainable power source for transport, stationary, and portable applications due to their high efficiency and low emissions.[1,2] Though tremendous progress has been made in the past decades, the slow kinetics of the oxygen reduction reaction (ORR) at the cathode of PEM fuel cells are still one of the primary aspects limiting its performance. To date, the best materials for the catalysis of ORR are platinum-based; however, they suffer from slow reduction kinetics and high cost, which hinders the large-scale commercialization of low-temperature fuel cells.[3–5] As a substitute for platinum, the development of nonprecious metal catalysts (NPMCs) with high activity and practical durability for ORR has been viewed as the long-term solution to reduce the cost.[6]

Much effort has been devoted to the development of NPMCs in recent years. Nonprecious metal/polymer nanocomposite catalysts with different nitrogen-containing precursors have demonstrated high catalytic activity toward ORR. Among these catalysts, NPMCs with high ORR activity synthesized by modification of the carbon support with porphyrin, polypyrrole, polyaniline, or ethylenediamine (EDA) as a nitrogen precursor has received a lot of attention.[7–13] However, most reports of NPMCs have not exceeded the performance of commercial platinum catalysts in PEM fuel cells in both activity and stability.

The major limitation to hindering the activity of NPMCs is its low catalytic active site density.[6,14] Two major approaches have been proposed to overcome the limitation: (1) synthesize a self-supported catalysts with a high surface area and (2) develop high surface area carbon supports with adequate pore sizes.[15] Many research papers discuss the performance of ORR catalysis by transition-metal compounds that are formed in nanopore structures, including the analysis of Fe-based catalysts by Dodelet and co-workers.[16] Dodelet et al. stated that two different catalytic sites, Me-N4-C (pyrrolic type) and Me-N2-C (pyridinic type), coexist in the catalysts, and these metal and nitrogen complexes bound to the carbon support is known to be catalytically active where the metal ion in the center of the macrosites plays a crucial role in ORR.[17–31] Recent papers published by Dodelet's group on the iron-based catalyst reported that the use of microporous carbon, Black Pearls 2000, has greatly increased the site density, leading to an increase in the catalytic activity for ORR.[32] It has been proposed that the Me-N-C catalytic sites consist of a metal cation coordinated by either two or four nitrogen functionalities and are located at the edges of the opposite walls of the carbon micropores.[33–35] Although there is controversy in the literature regarding the active site and mechanism to ORR catalysis for these NPMCs, it is commonly accepted that the key to achieving higher activity is to increase the metal−nitrogen complexes by increasing the surface concentration of nitrogen groups on the catalyst support. On the basis of these ideas, it can be concluded that there is

TABLE 1: Summary of Physical Properties of Ketjen Black EC300J and EC600JD

	KJ300	KJ600	FeCo-EDA-300R	FeCo-EDA-600R
BET surface area (m^2/g)	822.7	1416.2	298.1	483.7
pore volume (cm^3/g)	1.048	2.279	0.292	0.541
area from micropores (m^2/g)	154.23	591.89	28.42	136.11

* To whom correspondence should be addressed. E-mail: zhwchen@uwaterloo.ca.

10.1021/jp910138x
Published on Web 04/13/2010

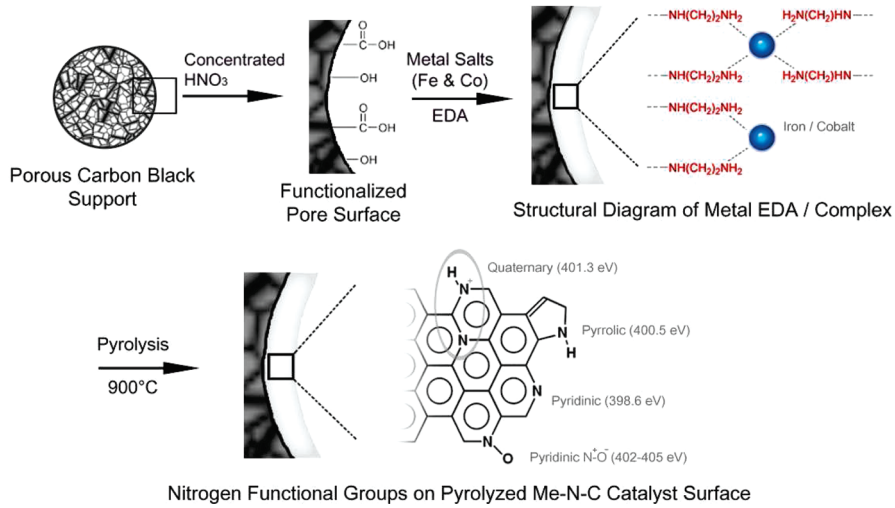

Figure 1. Schematic representation for the preparation of the FeCo-EDA-C catalyst.

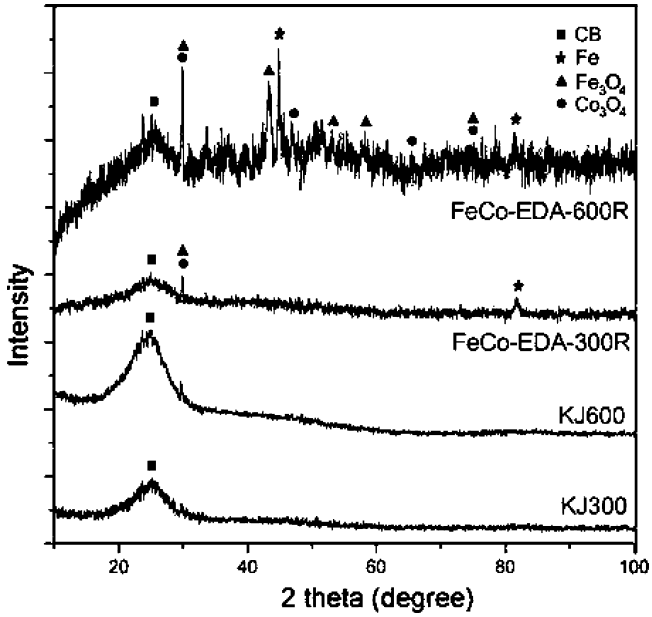

Figure 2. XRD patterns for functionalized KJ300, KJ600, FeCo-EDA-300R, and FeCo-EDA-600R.

great potential to improve catalytic activity if the surface-to-volume ratio of micropores on the carbon support can be increased.

In this study, high-performance NPMCs have been synthesized using Ketjen Black EC600JD (KJ600) as the carbon support, which possesses a much higher pore volume and Brunauer−Emmett−Teller (BET) surface area than that of the commonly used Ketjen Black EC300J (KJ300) support (Table 1). On both KJ300 and KJ600 supports, metal/nitrogen complexes are deposited using EDA, followed by a high-temperature pyrolysis step and chemical post-treatment. For metal additives, iron and cobalt are used as an agent to facilitate and stabilize the incorporation of nitrogen within the carbon matrix.[36] The schematic representation of the catalytic site formation in the pores of the carbon support is illustrated in Figure 1. The difference in ORR activity of the two catalysts will be discussed, and the relationship between the contents of different nitrogen groups present in the catalysts and the performance will be investigated.

TABLE 2: EDX Elemental Analysis of FeCo-EDA-300R and FeCo-EDA-600R Samples

composition	FeCo-EDA-300R (wt %)	FeCo-EDA-600R (wt %)
carbon	90.57	83.06
oxygen	4.73	4.72
iron	1.43	4.14
cobalt	1.04	4.31

Experimental Methods

Two different catalysts have been synthesized using KJ300 and KJ600 supports. Physical and electrochemical characterizations have been carried out on the sample catalyst products: FeCo-EDA-KJ300 and FeCo-EDA-KJ600. Two sets of samples were synthesized almost identically, the first set, which did not undergo a reflux process (FeCo-EDA-300 and FeCo-EDA-600), and the second set, which added a reflux during evaporation of ethanol (FeCo-EDA-300R and FeCo-EDA-600R), which show improved ORR activity over the samples synthesized without reflux.

Catalyst Synthesis. Two types of carbon black graphite, KJ300 and KJ600, were treated in concentrated (6 M) HCl solution to remove metal impurities present on the carbon. This was followed by thoroughly washing the carbon black with copious amounts of deionized water before filtering and drying the carbon black overnight in an oven at 60 °C. The remaining solid was subjected to reflux in 70% HNO_3 solution at 80 °C for 8 h to introduce carboxyl groups onto the carbon surface. The carbon black was then washed again with deionized water, filtered, and dried overnight in an oven at 60 °C. Both $Co(NO_3)_2 \cdot 6H_2O$ (0.25 g) and $FeSO_4 \cdot 7H_2O$ (0.25 g) were fully dissolved in 125 mL of ethanol before adding 2 mL of ethylenediamine. This solution was stirred for half an hour, thus creating the ethylenediamine polymer complex. Functionalized carbon black (0.5 g), which was synthesized previously, was then dispersed in 125 mL of ethanol and added with the metal and ethylenediamine polymer complex solution. The combined solution was then boiled for an hour under ambient pressure with and without reflux. This boiling procedure was done under air at approximately 80 °C in order to drive the polymerization. If reflux was used, it was then removed after an hour to allow the ethanol to evaporate completely. The remaining dried precipitate was ground and pyrolyzed at 900 °C for an hour, raising the temperature at 20 °C/min while supplying a constant flow of inert nitrogen gas. The sample was then acid-treated in

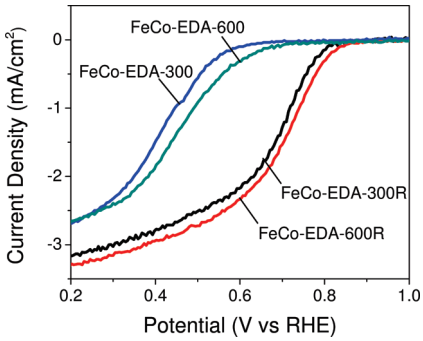

Figure 3. ORR curves of various catalysts, FeCo-EDA-300, FeCo-EDA-600, FeCo-EDA-300R, and FeCo-EDA-600R, obtained at 900 rpm in 0.5 M H_2SO_4.

TABLE 3: Half-Wave and Onset Potentials vs RHE of FeCo-EDA-300, FeCo-EDA-600, FeCo-EDA-300R, and FeCo-EDA-600R

	half-wave potential (V)	onset potential (V)
FeCo-EDA-300	0.43	0.68
FeCo-EDA-600	0.47	0.73
FeCo-EDA-300R	0.69	0.84
FeCo-EDA-600R	0.72	0.89

0.5 M H_2SO_4 for 8 h before being filtered and washed with 1 L of deionized water. The sample was oven-dried overnight at 80 °C before use.

Physical Characterization. The surface areas and pore properties of these materials were obtained on a Micromeritics ASAP-2020 analyzer. The samples were degassed at 250 °C, and nitrogen was adsorbed on the carbon catalyst and perovskite powders at liquid nitrogen temperature (−196 °C). The surface area and pore volume were determined by conventional BET and BJH equations using adsorption data. X-ray diffraction (XRD) data were obtained by using an Inel XRG 3000 with Cu Kα radiation to determine elemental composition of the catalysts. Energy-dispersive X-ray spectroscopy (EDX) data were obtained by using a LEO1530 FE-SEM, equipped with an EDAX Pegasus 1200 integrated EDX/OIM. X-ray photoelectron spectroscopy (XPS) data were obtained using a Thermal Scientific K-Alpha XPS spectrometer in order to investigate the relative content of different elements in the catalyst sample.

Electrocatalytic Activity Evaluation. The electrocatalytic activity was evaluated in a three-electrode electrochemical cell using a Pine-Instrument's Bipotentiostat AFCBP1, equipped with a speed rotator. The electrode was equipped with a 0.19635 cm^2 glassy carbon surface and a 5.0 mm diameter Pt ring (collection efficiency of 26%). All RRDE measurements were performed in acidic electrolyte, 0.5 M H_2SO_4, using a Ag/AgCl reference electrode at room temperature. To prepare the electrode, 4 mg of sample was dissolved ultrasonically into 2 mL of ethanol before 20 μL of the ink and 10 μL of 0.05% Nafion solution were applied to the glassy carbon disk. Thus, the catalyst loading on the glass carbon electrode was approximately 0.204 mg/cm^2. ORR curves were recorded in the potential range at a scan rate of 10 mV/s with the electrolyte saturated with oxygen gas. ORR curves were corrected for the background by conducting the same sweep voltammetry in the absence of oxygen and subtracting the curve from the measured ORR curves. Nitrogen was used as the inert gas, which was with saturated in the electrolyte. The measurements were repeated at various rotation speeds (100, 400, 900, and 1600 rpm). The ring potential was maintained at 1.2 V versus RHE throughout the experiments in order to oxidize H_2O_2 produced during oxygen reduction on disk electrode.

MEA Preparation. A commercially available catalyzed GDE (LT250EW Low Temperature ELAT GDE Microporous Layer, E-TEK) was used as the anode for the fuel cell test. Cathode catalyst ink was prepared by thoroughly blending the FeCo-EDA-600R composite catalyst with deionized water and recast Nafion ionomer (5% Nafion suspension in alcohols, 1100 Nafion equivalent weight, Solution Technology, Inc.). The catalyst was combined with deionized water to achieve a 1:10 ratio by weight. The Nafion suspension was added in an amount sufficient to reach a 1:1 volumetric ratio between the ionically conducting phase (Nafion) and the electronically conducting phase (catalyst + carbon) in dry cathode catalyst. The mixture was placed in an ice bath to prevent overheating and minimize evaporation of solvents and then ultrasonically mixed for 100 s. A piece of a Nafion 212 membrane was placed on the top of a vacuum table preheated to 80 °C. The vacuum table was used to hold the membrane in place and avoid wrinkling during the catalyst application. Cathode ink was then applied to one side of the membrane using a camel hair brush. Upon completion of the painting, the MEA was left on the heated vacuum table for an additional 30 min to allow the cathode catalyst layers to cure. The MEA was then removed from the table and placed in a sealed plastic bag for future use. The cathode catalyst loadings were 4.0 mg/cm^2.

Fuel Cell Polarization Measurements. The MEA was assembled in a 5 cm^2 fuel cell prototype. Hydrophobic double-sided gas diffusion layers "backings" from De Nora USA/E-TEK Inc. were used on the cathode of the MEA. The MEAs were conditioned in hydrogen−oxygen at 0.40 V and 80 °C. The conditioning was continued until the current density reached a constant level. The flow rates of hydrogen and oxygen were 2 and 5 mL/s, respectively. The anode and cathode gases were humidified at 90 and 80 °C, respectively. Back pressures of the H_2/O_2 during the polarization were set to 30 psi/30 psi, while no back pressures were set for the durability tests.

Results and Discussion

XRD patterns for the two carbon black supports and FeCo-EDA complex catalysts based on those supports are shown in Figure 2. All samples showed broad carbon peaks at $2\theta = 24.3°$. It can be seen that the carbon peak in the KJ600 sample is more distinct than that of KJ300.[37] Although the XRD result for the FeCo-EDA-300R catalyst shows evidence of iron and cobalt oxides, the intensity and variety of the peaks representing transition metals in FeCo-EDA-600R are far more distinct. It was hypothesized that, even if the same amount of both KJ300 and KJ600 supports are used, the KJ600 support provides a much higher surface area to be combined with polymer structure and is able to capture greater amounts of those excess polymer metal composites that KJ300 supports cannot. The graph obtained for FeCo-EDA-600R shows distinct iron and iron oxide peaks ($2\theta = 44.7$, 51.9, 76.4, and 82.3°) and cobalt oxide peaks ($2\theta = 32.4$, 48.3, 64.5, and 73.1°), which verifies the presence of iron- and cobalt-containing crystalline phases.[37,38] The elemental analysis carried out by EDX is summarized in Table 2. Both samples contain approximately the same amount of oxygen but differ in the weight percent of both iron and cobalt. The weight percent of iron and cobalt in the FeCo-EDA-600R catalyst is approximately 3−4 times higher than that of FeCo-EDA-300R, which supports the argument that the KJ600 support has better capability as a catalyst support to combine with polymer complex due to its larger surface area and pore volume. From Table 1, KJ600 has almost double the surface area (1416.2 m^2/g) and higher pore volume (2.279 cm^3/g) and micropore area

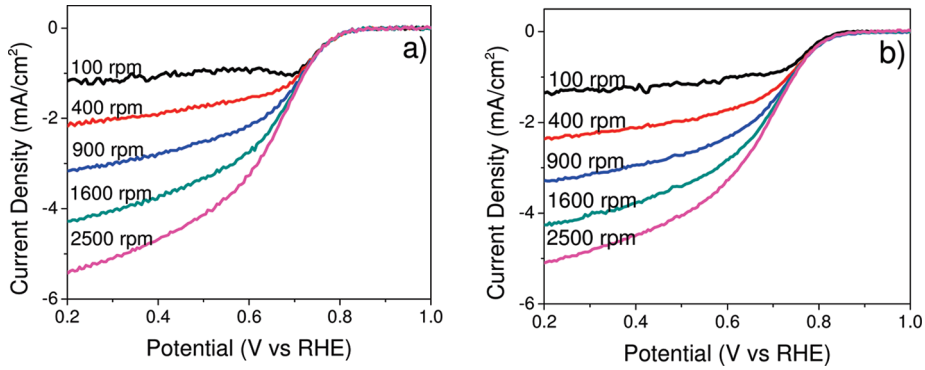

Figure 4. ORR curves of (a) FeCo-EDA-300R and (b) FeCo-EDA-600R at various rotation speeds in 0.5 M H_2SO_4 electrolyte.

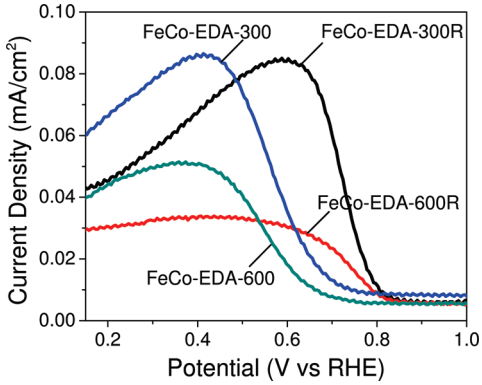

Figure 5. Hydrogen peroxide yield for various catalysts obtained at 900 rpm in 0.5 M H_2SO_4: FeCo-EDA-300, FeCo-EDA-600, FeCo-EDA-300R, and FeCo-EDA-600R.

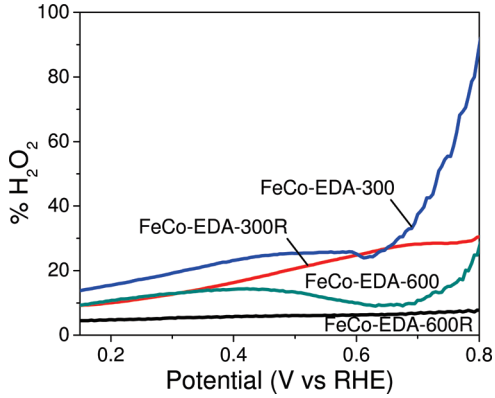

Figure 6. Fractional yield of hydrogen peroxide for four samples, FeCo-EDA-300, FeCo-EDA-600, FeCo-EDA-300R, and FeCo-EDA-600R, obtained at 900 rpm in 0.5 M H_2SO_4.

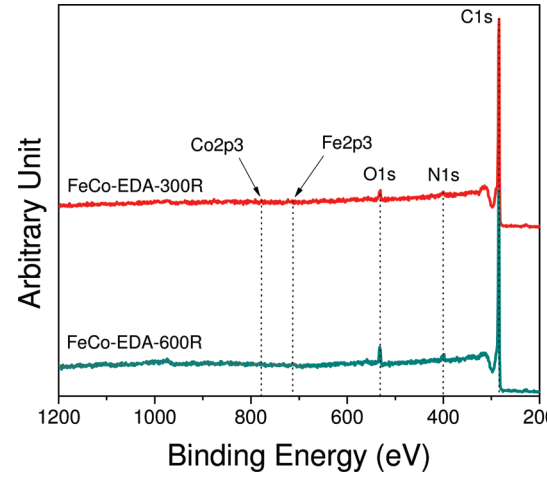

Figure 7. XPS spectrum of FeCo-EDA-300R and FeCo-EDA-600R showing all the elements in the samples.

TABLE 4: XPS Analysis of the Elemental Composition of FeCo-EDA-300R and FeCo-EDA-600R

	FeCo-EDA-300R		FeCo-EDA-600R	
	peak position (eV)	atom %	peak position (eV)	atom %
carbon	~284.36	96.25	~284.48	94.33
nitrogen	~400.01	1.66	~400.74	2.18
oxygen	~531.24	2.09	~532.13	3.49

(591.89 m^2/g) of KJ300, which can lead to a significant increase in performance of the resulting catalysts. After insertion and impregnation of the carbon support by the FeCo-EDA complex and the subsequent heat and chemical treatments, the areas of micropores of FeCo-EDA-300R and FeCo-EDA-600R decreased to 28.42 and 136.11 m^2/g, respectively. The same also applies to the total pore volume and BET surface area, where the catalytic materials clog the pores, leading to a total decrease of the available pore volumes.

The electrocatalytic activity of the four catalysts was evaluated using rotating RRDE voltammetry, shown in Figure 3. The half-wave potential and onset potential of each catalyst are summarized in Table 3. The onset potential was measured by taking the potential at which the ORR curves deviated from 0 current from ORR curves corrected for the background. This correction was made by obtaining ORR curves at 100, 400, 900, and 1600 rpm in oxygen-saturated conditions and subtracting the background current, which was obtained by conducting the voltammetry under nitrogen-saturated electrolyte conditions. Similarly, the half-wave potential was measured by finding the potential that was halfway between the limiting current (measured at 0.2 V vs RHE) and zero current on the ORR voltammetry curve. The FeCo-EDA-600R shows the best performance, followed by FeCo-EDA-300R, FeCo-EDA-600, and FeCo-EDA-300. From ORR curves, the effect of the refluxing process on the electrocatalytic activity is very clear. Refluxing contributed to the half-wave and onset potentials being about 0.25 and 0.15 V higher, respectively. This phenomenon is due to the longer polymerization period allowing the uniformity coating of FeCo-EDA complex into the nanoporous structure of carbon supports. For both types of samples that have been synthesized without reflux and with reflux, it can also be concluded that the use of the KJ600 support improves the catalytic activity of the samples. Compared to KJ300-based catalysts, the half-wave and onset potentials of KJ600-based catalysts are shifted to the positive side (average increase of 0.03 and 0.04 V, respectively), indicating better electrocatalytic activity due to the increase in the active surface area. On the

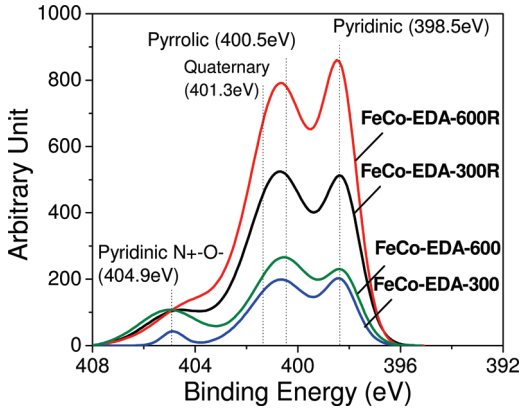

Figure 8. XPS spectrum showing the presence of different types of nitrogen groups from the N 1S signal.

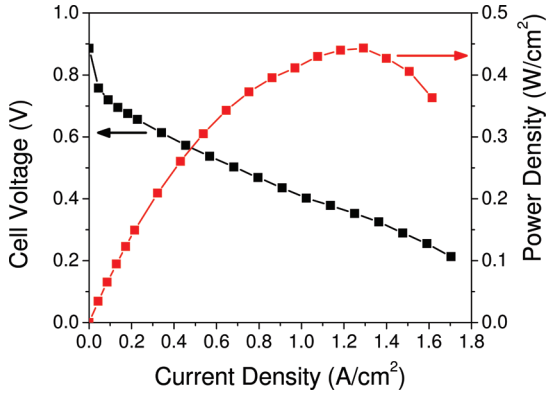

Figure 9. Polarization curve and corresponding power densities of MEAs fabricated with the FeCo-EDA-KJ600R cathode catalyst and commercially available catalyzed GDE anode. Cell temperature, 80 °C; catalyst loading, 4 mg/cm^2; H_2/O_2 back pressures, 30 psi/30 psi.

basis of these results, it can be concluded that there is a great potential to improve catalytic activity if the area of micropores, pore volume, and surface are of the carbon support can be increased. ORR curves obtained at various rotating speeds for FeCo-EDA-300R and FeCo-EDA-600R are shown in Figure 4.

The RRDE voltammetry curves showing the amount of hydrogen peroxide generated during the ORR process of four samples are illustrated in Figure 5. The current density, which is directly related to the amount of hydrogen peroxide, obtained for KJ300-based catalysts are almost twice that of the KJ600-based catalysts. Between the two KJ600-based ones, FeCo-EDA-600R showed the best oxygen reduction activity and generated the least amount of hydrogen peroxide during the reaction. The fractional yield of hydrogen peroxide for each sample has been determined and illustrated in Figure 6. Figure 6 shows that KJ300-based catalysts have a fractional yield ranging from approximately 10 to 20%, whereas the values for KJ600-based catalysts fall in the range of 5−10%. FeCo-EDA-600R showed the lowest fractional yield of 5%. These results indicated that the activity and selectivity of NPMCs could be improved by using higher pore volume and surface area carbon as the catalyst support.

The elemental composition and different structural groups of nitrogen in FeCo-EDA-300R and FeCo-EDA-600R were obtained using XPS, shown in Figure 7 and Table 4. From XPS results, FeCo-EDA-600R showed a higher nitrogen content (2.15 atom %) compared with FeCo-EDA-300R (1.65 atom %). It is expected that the FeCo-EDA-600R catalyst has a higher nitrogen

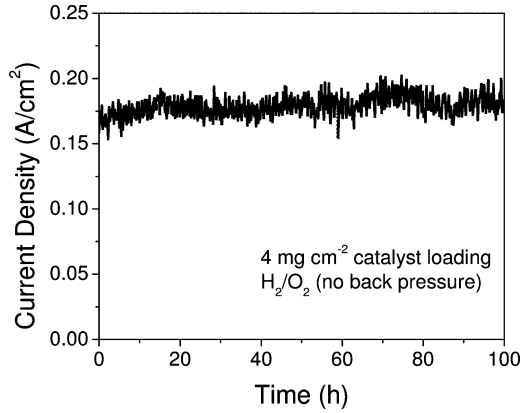

Figure 10. Durability test of the H_2/O_2 PEM fuel cell at 0.4 V for 100 h. MEA was fabricated with the FeCo-EDA-KJ600R catalyst and commercially available catalyzed GDE as the cathode and anode, respectively. Cathode catalyst loading, 4 mg/cm^2; cell temperature, 80 °C; no back pressure.

content, which could lead to better catalytic activity for various fuel cell catalysts.[39] Further analysis has been carried out on the N 1S signal, and the data for all four samples have been plotted in Figure 8. Three distinct peaks are observed, centered at 404.9, 400.7, and 398.3 eV for each catalyst. The peaks at 404.9 and 398.3 eV are known as pyridinic N^+-O^- and pyridinic nitrogen groups, respectively, whereas there is some uncertainty regarding the peak at 400.7 eV because it is close to both the peak of the pyrrolic nitrogen group at 400.5 eV and the peak of the quaternary nitrogen group at 401.3 eV. In this report, the middle peak will be considered as the coexistence of both pyrrolic and quaternary nitrogen groups. The graph clearly shows that, for the FeCo-EDA catalyst, the amount of nitrogen content (which can be determined by calculating the area under the curves) is directly related to the electrocatalytic performance. Although the contribution to the catalytic activity of the pyridinic N^+-O^- nitrogen groups seems ambiguous, it is hypothesized that pyrrolic/quaternary and pyridinic peaks lead to formation of complex structures that are better suited as catalysts. From Figure 8, it can be observed that the amplitude of the pyridinic peak is rising as the catalyst performance is increased compared to the other nitrogen peaks. It has been studied that the formation of pyridinic nitrogen groups is observed on the edge of the graphite plane and the lone pair of electrons from pyridinic nitrogen groups has been attributed to be ORR active.[40] The higher exposure of the planar edges of graphite in FeCo-EDA-600R due to the more rugged surface structure is expected to expose more pyridinic nitrogen, which enhances ORR activity. For these reasons, it is expected that the ORR activity of FeCo-EDA-600R is greatest.

To evaluate the ORR catalytic activity of the FeCo-EDA-600R catalyst in practical fuel cell applications, an MEA was fabricated with the catalyst at the cathode and tested using a fuel cell test station. The PEM fuel cell polarization curve was obtained at 80 °C using a 30 psi back pressure for both H_2 and O_2. The polarization curves and the corresponding power density curves are shown in Figure 9. At a cell voltage of 0.6 V, the current density is 0.37 A/cm^2 with a maximum power density of 0.44 W/cm^2. The stability of the FeCo-EDA-600R catalyst material was tested by holding the cell voltage at 0.4 V at 80 °C for 100 h. No back pressure was applied to the MEA, and the cathode catalyst loading was 4.0 mg/cm^2. Figure 10 graphically depicts this current transient for the H_2/O_2 cell with no visible degradation in performance.

Conclusions

Nonprecious metal catalysts were developed by in situ polymerization of ethylenediamine with iron and cobalt on two different porous carbon black supports in order to improve ORR activity. Among those materials, the FeCo-EDA-600R catalyst possesses the highest electrochemical activity for ORR, as well as the least amount of hydrogen peroxide generated at approximately 5%. Between the two carbon graphite catalyst supports, KJ300 and KJ600, KJ600 showed greater potential in generating higher catalytic activity when used as a nonprecious metal catalyst due to its higher pore volume and surface area. During synthesis, KJ600 leads to a higher nitrogen content, providing more active sites for ORR. When a nonprecious metal catalyst is synthesized using this in situ method, giving enough time for the polymerization of FeCo-EDA complex into the nanopores is a critical parameter that leads to noticeable improvements in ORR performance. The MEA fabricated with the FeCo-EDA-KJ600R catalyst maintained high power densities. At a cell voltage of 0.3 V, a current density of 1.4 A/cm^2 was achieved with a maximum power density of 0.44 W/cm^2. Further study will be necessary to determine the durability of the MEA in fuel cell operating conditions. However, it can be concluded that a higher pore volume and surface area of the carbon support could lead to a higher nitrogen content, providing more active sites for ORR, and this type of catalyst has great potential used as a nonprecious PEM fuel cell catalyst.

Acknowledgment. This work was financially supported by the Natural Sciences and Engineering Research Council of Canada (NSERC) and the University of Waterloo.

References and Notes

(1) Bezerra, C.; Zhang, L.; Lee, K.; Liu, H.; Marques, A.; Marques, E.; Wang, H.; Zhang, J. *Electrochim. Acta* **2008**, *53*, 4937.
(2) Hermann, A.; Chaudhuri, T.; Spagnol, P. *Int. J. Hydrogen Energy* **2005**, *30*, 1297.
(3) Lee, K.; Zhang, L.; Lui, H.; Hui, R.; Shi, Z.; Zhang, J. *Electrochim. Acta* **2009**, *54*, 4704.
(4) Li, X.; Park, S.; Popov, B. *J. Power Sources* **2010**, *195*, 445.
(5) Zhang, L.; Zhang, J.; Wilkinson, D.; Wang, H. *J. Power Sources* **2006**, *156*, 171.
(6) Wood, T.; Tan, Z.; Schmoeckel, A.; O'Neill, D.; Atanasoski, R. *J. Power Sources* **2008**, *178*, 510.
(7) Barsukov, V.; Khomenko, V.; Chivikov, S.; Barsukov, I.; Motronyuk, T. *Electrochim. Acta* **2001**, *46*, 4083.
(8) Barsukov, V.; Khomenko, V.; Katashinskii, A.; Motronyuk, T. *Russ. J. Electrochem.* **2004**, *40*, 1170.
(9) Khomenko, V.; Barsukov, V.; Katashinskii, A. *Electrochim. Acta* **2005**, *50*, 1675.
(10) Martínez Millán, W.; Toledano Thompson, T.; Arriaga, L.; Smit, M. *Int. J. Hydrogen Energy* **2009**, *34*, 694.
(11) Subramanian, N.; Kumaraguru, S.; Colon-Mercado, H.; Kim, H.; Popov, B.; Black, T.; Chen, D. *J. Power Sources* **2006**, *157*, 56.
(12) Wu, G.; Chen, Z.; Artyushkova, K.; Garzon, F.; Zelenay, P. *ECS Trans.* **2008**, *16*, 159.
(13) Zhou, Q.; Li, C.; Li, J.; Lu, J. *J. Phys. Chem. C* **2008**, *112*, 18578.
(14) Zhang, L.; Lee, K.; Bezerra, C.; Zhang, J. *Electrochim. Acta* **2009**, *54*, 6631.
(15) Liu, H.; Song, C.; Tang, Y.; Zhang, J. *Electrochim. Acta* **2007**, *52*, 4532.
(16) Lefevre, M.; Dodelet, J.; Bertrand, P. *J. Phys. Chem. B* **2000**, *104*, 11238.
(17) Schulenburg, H.; Stankov, S.; Schunemann, V.; Radnik, J.; Dorbandt, I.; Fiechter, S.; Bogdanoff, P.; Tributsch, H. *J. Phys. Chem. B* **2003**, *107*, 9034.
(18) Bashyam, R.; Zelenay, P. *Nature* **2006**, *443*, 63.
(19) Marcotte, S.; Villers, D.; Guillet, N.; Roue, L.; Dodelet, J. *Electrochim. Acta* **2004**, *50*, 179.
(20) Widelov, A.; Larsson, R. *Electrochim. Acta* **1992**, *37*, 187.
(21) Yamazaki, S.; Yamada, Y.; Ioroi, T.; Fujiwara, N.; Siroma, Z.; Yasuda, K.; Miyazaki, Y. *J. Electroanal. Chem.* **2005**, *576*, 253.
(22) Villers, D.; Jacques-Bédard, X.; Dodelet, J. *J. Electrochem. Soc.* **2004**, *151*, A1507.
(23) Gojkovi, S.; Gupta, S.; Savinell, R. *J. Electroanal. Chem.* **1999**, *462*, 63.
(24) Sawai, K.; Suzuki, N. *J. Electrochem. Soc.* **2004**, *151*, A682.
(25) Sawai, K.; Suzuki, N. *J. Electrochem. Soc.* **2004**, *151*, A2132.
(26) Cote, R.; Lalande, G.; Guay, D.; Dodelet, J.; Denes, G. *J. Electrochem. Soc.* **1998**, *145*, 2411.
(27) Lalande, G.; Cote, R.; Guay, D.; Dodelet, J.; Weng, L.; Bertrand, P. *Electrochim. Acta* **1997**, *42*, 1379.
(28) Yuasa, M.; Yamaguchi, A.; Itsuki, H.; Tanaka, K.; Yamamoto, M.; Oyaizu, K. *Chem. Mater.* **2005**, *17*, 4278.
(29) Gouerec, P.; Savy, M. *Electrochim. Acta* **1999**, *44*, 2653.
(30) Gouerec, P.; Savy, M.; Riga, J. *Electrochim. Acta* **1998**, *43*, 743.
(31) Jaouen, F.; Charreteur, F.; Dodelet, J. *J. Electrochem. Soc.* **2006**, *153*, A689.
(32) Lefevre, M.; Proietti, E.; Jaouen, F.; Dodelet, J. *Science* **2009**, *324*, 71.
(33) Charreteur, F.; Jaouen, F.; Ruggeri, S.; Dodelet, J. *Electrochim. Acta* **2008**, *53*, 2925.
(34) Jaouen, F.; Lefevre, M.; Dodelet, J.; Cai, M. *J. Phys. Chem. B* **2006**, *110*, 5553.
(35) Jaouen, F.; Dodelet, J. *J. Phys. Chem. C* **2007**, *111*, 5963.
(36) Nallathambi, V.; Lee, J.; Kumaraguru, S.; Wu, G.; Popov, B. *J. Power Sources* **2008**, *183*, 34.
(37) Gupta, K.; Jana, P.; Meikap, A. *J. Phys. Sci.* **2008**, *12*, 233.
(38) Hong, Y.; Rheem, Y.; Lai, M.; Cwiertny, D.; Walker, S.; Myung, N. *Chem. Eng. J.* **2009**, *151*, 66.
(39) Liu, J.; Czerw, R.; Carroll, D. *J. Mater. Res.* **2005**, *20*, 538.
(40) Maldonado, S.; Morin, S.; Stevenson, K. *Carbon* **2006**, *44*, 1429.

JP910138X